Local thermal expansions and lattice strains in Elinvar and stainless steel alloys

Toshihiko Yokoyama,* Akihiro Koide,† and Yohei Uemura
Department of Materials Molecular Structure, Institute for Molecular Science, Myodaiji-cho, Okazaki, 444-8585, Japan

(Received 14 December 2017; published 13 February 2018)

Local thermal expansions and lattice strains in the Elinvar alloy $Fe_{49.66}Ni_{42.38}Cr_{5.49}Ti_{2.47}$ (Ni Span C) and the stainless steel SUS304 $Fe_{71.98}Ni_{9.07}Cr_{18.09}Mn_{0.86}$ (AISI304) were investigated by the temperature-dependent Cr, Fe, and Ni K-edge extended x-ray absorption fine-structure (EXAFS) measurements, combined with the path-integral effective classical potential Monte Carlo (PIECP MC) theoretical simulations. From the EXAFS analysis of the Elinvar alloy, the local thermal expansion around Fe is found to be considerably smaller than the ones around Ni and Cr. This observation can be understood simply because Fe in the Elinvar alloy exhibit an incomplete Invar-like effect. Moreover, in both the Elinvar and SUS304 alloys, the local thermal expansions and the lattice strains around Cr are found to be larger than those around Fe and Ni. From the PIECP MC simulations of both the alloys, the first-nearest neighbor Cr-Fe pair shows extraordinarily large thermal expansion, while the Cr-Cr pair exhibits quite small or even negative thermal expansion. These findings consequently indicate that the lattice strains in both the Elinvar and SUS304 alloys are concentrated predominantly on the Cr atoms. Although the role of Cr in stainless steel has been known to inhibit corrosion by the formation of surface chromium oxide, the present investigation may interestingly suggest that the Cr atoms in the bulk play a hidden new role of absorbing inevitable lattice strains in the alloys.

DOI: 10.1103/PhysRevMaterials.2.023601

I. INTRODUCTION

It is well known that local structures in mixed crystals are often different from lattice structures that are expected crystallographically [1–4]. Even when the crystal shows clear x-ray diffraction patterns, there should exist strains in the crystal that cannot be solved by the x-ray diffraction analysis. In metallic alloys as well, our previous extended x-ray absorption fine structure (EXAFS) studies on the Invar alloy $Fe_{64}Ni_{36}$ [5] and the martensite alloy $Mn_{88}Ni_{12}$ [6], the local structures, are meaningfully different between the different metal atoms in these binary alloys, although both the alloys exhibit quite normal x-ray diffraction patterns of fcc lattices and both the metal atoms should crystallographically be identical. Moreover, the local thermal expansions were found not to be identical; in the Invar alloy, the local structure around Fe shows almost no local thermal expansion due to the so-called Invar effect [7,8], while the Ni K-edge EXAFS provides small but meaningful thermal expansion around Ni. It is thus important to determine local structures as well as periodic structures directly for the detailed understanding of lattice strains in the crystal.

The Elinvar alloy is a unique material that shows temperature invariance of the Young modulus or other elastic constants for a wide temperature range and has been applied to various practical precision mechanical equipments. Figures 1 and 2 depict temperature dependence of the Young moduli [9] and the lattice constant (divided by $\sqrt{2}$) [10] of the Elinvar alloy, together with the Invar alloy, Ni, Cu, stainless steel SUS304 (AISI304), etc. The Young moduli of normal materials such as Ni, Cu, and SUS304 in Fig. 1 gradually decrease with the temperature rise because of vibrational anharmonicity. On the contrary, the Invar alloy exhibits an increase in the Young modulus with the temperature. As shown in Fig. 2, the Invar alloy provides almost no thermal expansion for a wide temperature range from 0 to 400 K, which is the so-called Invar effect. The Invar effect can simply be understood in the following manner. In the Invar alloy, there exist at least two types of Fe atoms; one is an energetically unstable antiferromagnetic (AFM) Fe with a smaller atomic radius and the other is a stable ferromagnetic (FM) Fe with a larger atomic radius. Thermodynamically, the composition ratio of FM Fe decreases with the temperature rise, leading to the thermal contraction of the interatomic distance. This contraction can compensate for the normal thermal expansion due to vibrational anharmonicity, resulting in invariance of the interatomic distance in the Invar alloy. Since the AFM Fe atom interacts more strongly with neighboring atoms than the FM one, the Young modulus is resultantly enhanced at higher temperature. As shown in Figs. 1 and 2, the Elinvar alloy gives intermediate properties concerning both the Young modulus and the thermal expansion due to an incomplete Invar-like effect. As a result, the Young modulus of the Elinvar alloy exhibits almost no temperature dependence above ∼100 K.

In Figs. 1 and 2 the Young modulus and the thermal expansion of stainless steel SUS304 (AISI304) are also depicted. Stainless steel is one of the most practically useful metals in our daily lives. Here chromium is the key element that inhibits corrosion of stainless steel by the formation of rigid surface chromium oxide layers. For solid-state properties of austenite stainless steel with fcc structure as SUS304, Cr plays

*yokoyama@ims.ac.jp
†Present address: Département Matériaux-Nanosciences, Institut de Physique de Rennes, UMR UR1-CNRS 6251, Universite de Rennes1, 35042 Rennes-cedex, France

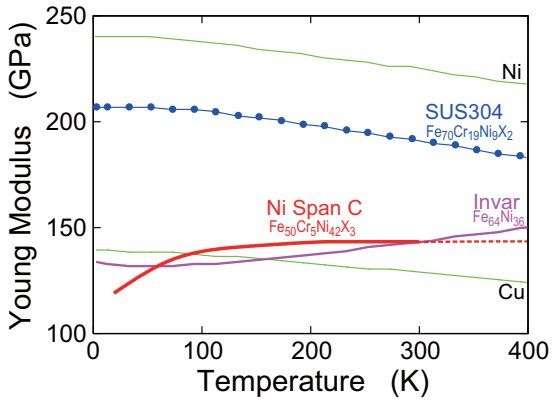

FIG. 1. Temperature dependence of the Young modulus of the Elinvar alloy (Ni Span C), together with those of the Invar alloy, SUS304, Ni, and Cu.

a role of making the alloy antiferromagnetic. Although the Young modulus of SUS304 in Fig. 1 shows a rather normal behavior, the thermal expansion in Fig. 2 should be noted to be pretty large compared with elemental Fe and Cr that configure SUS304. This is because fcc SUS304 has weaker metallic bonding due to a larger coordination number than bcc Fe and Cr.

In the present study we have investigated temperature dependence of the local structures of the Elinvar and SUS304 alloys by the combined techniques of Cr, Fe, and Ni K-edge EXAFS analysis and the theoretical simulations based on the path-integral effective classical potential Monte Carlo (PIECP MC) method [5,6,11,12] that approximately includes the vibrational quantum effect indispensable for the description of thermal and structural properties of solids at low temperature without huge computational loads. The first purpose of the present investigation is to clarify whether the local thermal expansion is identical to the lattice thermal expansion. In the previous binary Invar [5] and MnNi [6] alloys, the local thermal expansions differ significantly from the lattice expansion, because one metal element (Fe in $Fe_{64}Ni_{36}$ and Mn in $Mn_{88}Ni_{12}$) exhibit the transformation of the electronic states depending on temperature. In the present ternary alloys, the

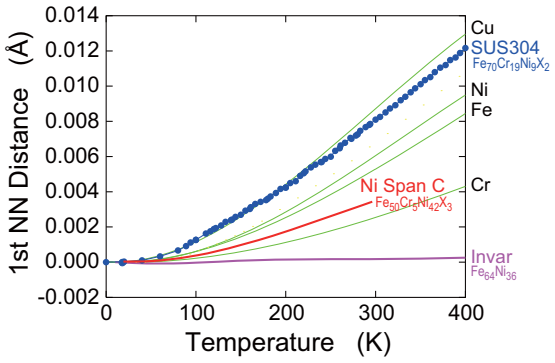

FIG. 2. Temperature dependence of the first-nearest neighbor interatomic distance (lattice constant divided by $\sqrt{2}$) of the Elinvar alloy (Ni Span C), together with those of the Invar alloy, SUS304, Cr, Fe, Ni, and Cu.

local thermal expansion around Fe in the Elinvar alloy may be different from the lattice one as in the case of Fe in the Invar alloy. Here we will focus our attention on the local thermal expansions not only for Fe in the Elinvar alloy but also for the other elements in both the alloys. The second purpose is to elucidate the lattice strains in the Elinvar and SUS304 alloys. In the present EXAFS analysis, we find that the local structure around Cr is significantly different from the other ones in both the alloys and that the lattice strain is concentrated dominantly around Cr. Although EXAFS reveals the difference in the local structures around the x-ray absorbing atoms, information on the surrounding atoms should be limited; only the average can be obtained in the present cases because it is difficult to distinguish the surrounding scattering atoms of Fe, Ni, or Cr with similar atomic numbers. We will clarify by the PIECP MC theoretical simulations the behaviors of all the atom pairs in both the Elinvar and SUS304 alloys.

The present article is organized as follows. In Sec. II experimental and theoretical methods are described in detail. Section III deals with the results and discussion, in which the local thermal expansions and strains around Fe, Ni, and Cr atoms are described separately, mainly based on the temperature-dependent EXAFS analysis. As the PIECP MC simulations are found to be in good agreement with the experimental EXAFS results, further details concerning the local thermal expansions and strains for each atom pairs are consequently discussed. In Sec. IV, concluding remarks and the summary of the present investigation are consequently presented.

II. EXPERIMENT AND THEORY

A. EXAFS

An Elinvar alloy $Fe_{49.66}Ni_{42.38}Cr_{5.49}Ti_{2.47}$ (Ni Span C) with 15.0 μm thickness and a SUS304 alloy $Fe_{71.98}Ni_{9.07}Cr_{18.09}Mn_{0.86}$ (AISI304 stainless steel) with 10.5 μm thickness were purchased from Sugiyama Metals Co., Ltd. in Osaka, Japan. The Cr, Fe, and Ni K-edge EXAFS spectra of the alloys were recorded at Beamline 9C of Photon Factory (the electron storage ring energy of 2.5 GeV and the ring current of 450–250 mA) in High Energy Accelerator Research Organization (KEK-PF) [13] with the transmission mode using a Si(111) double crystal monochromator. Ionization chambers filled with 30% N_2 in He and 100% N_2 were used to measure the incident and transmitted x-ray intensities, respectively. The samples were cooled down using a He gas-circulating refrigerator and the measurement temperature range was 20–300 K. For the Cr and Fe K-edge measurements, the monochromator crystals were detuned by 30% to eliminate the third-order harmonics, while for the Ni K-edge measurements the detuning process was not conducted. The Cr K-edge EXAFS measurements were terminated at the Mn K edge because of the presence of small amounts of Mn in both the alloys, while the Fe and Ni K-edge EXAFS were successfully recorded over sufficiently wide energy ranges due to the absence of Co and Cu impurities.

The EXAFS oscillation functions $k^3\chi(k)$ (k the photoelectron wave number) were obtained based on the standard procedures as the pre-edge baseline and the post-edge background subtractions and the subsequent normalization with atomic ab-

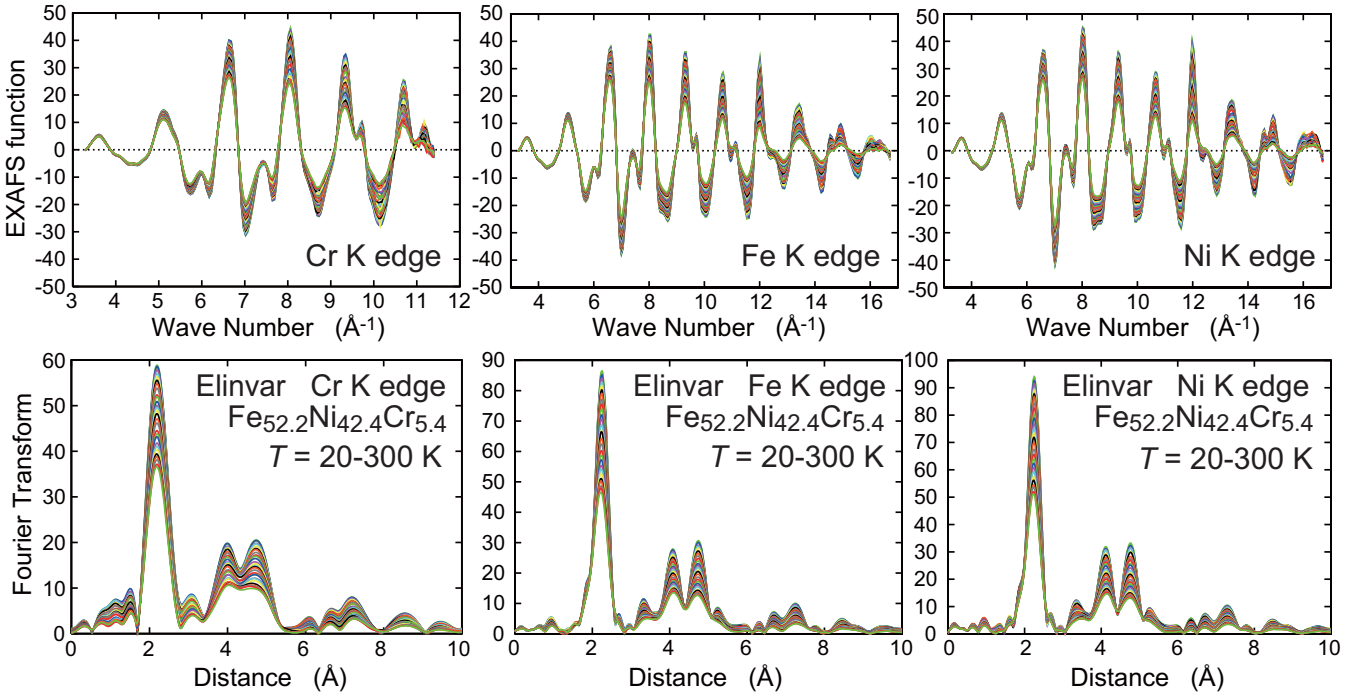

FIG. 3. Cr, Fe, and Ni K-edge EXAFS functions $k^3\chi(k)$ and their Fourier transforms of the Elinvar alloy at 20–300 K.

sorption coefficients. The $k^3\chi(k)$ functions were subsequently Fourier transformed, Fourier filtered for the peaks of interest, and were finally curve fitted in k space. In the present study, only the first nearest neighbor (NN) shells were quantitatively analyzed. The k and R spaces employed are summarized in Table I, and the $k^3\chi(k)$ functions and their Fourier transforms of the Elinvar and SUS304 alloys are depicted in Figs. 3 and 4, respectively.

The single-shell EXAFS formula employed is given as

$$\chi(k) = \frac{S_0^2 N F(k)}{kR^2} \exp[-2C_2k^2] \sin\left[2kR + \phi(k) - \frac{4}{3}C_3k^3\right], \tag{1}$$

where N is the coordination number, R is the interatomic distance, C_2 is the mean square relative displacement

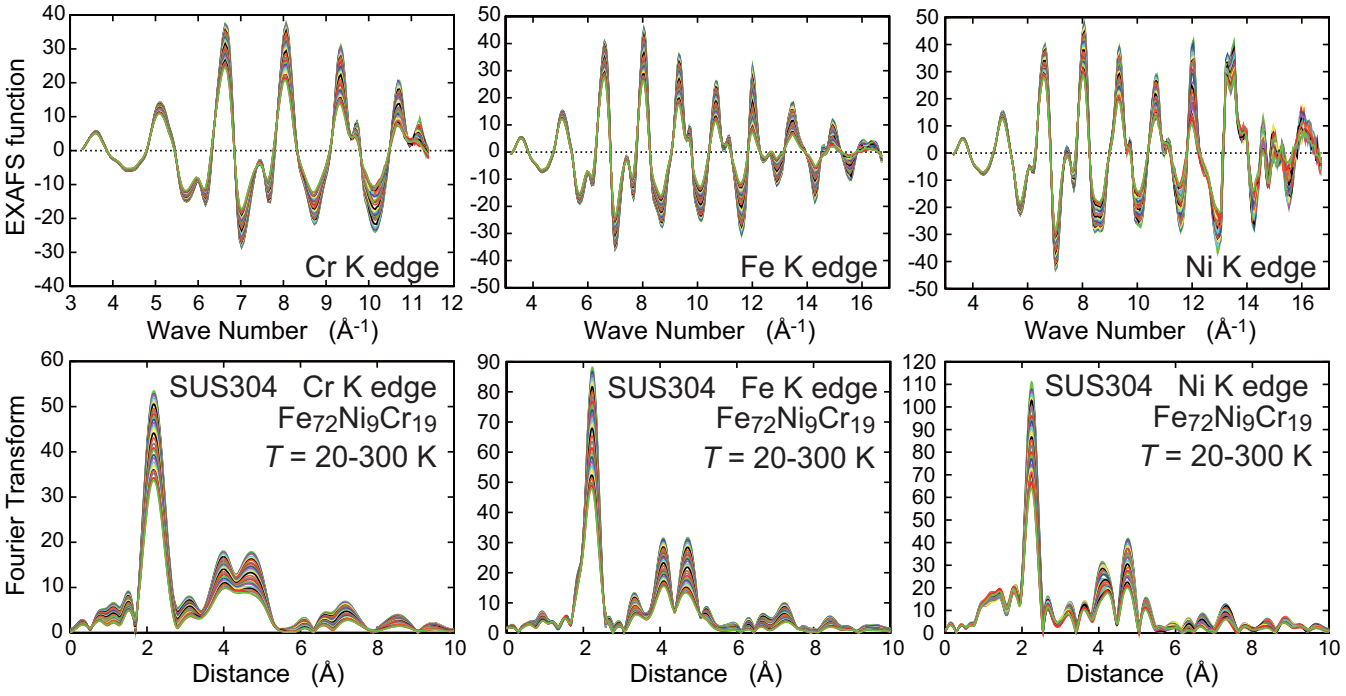

FIG. 4. Cr, Fe, and Ni K-edge EXAFS functions $k^3\chi(k)$ and their Fourier transforms of the SUS304 alloy at 20–300 K.

TABLE I. k and R ranges employed in the present EXAFS analysis. $\Delta k_{\rm FT}$ denotes the k range in the Fourier transform, $\Delta R_{\rm fit}$ is the R range in the Fourier filtering, and $\Delta k_{\rm fit}$ is the curve-fitting k range.

Sample	Edge	$\Delta k_{\rm FT}$ (Å^{-1})	$\Delta R_{\rm fit}$ (Å)	$\Delta k_{\rm fit}$ (Å^{-1})
Elinvar	Cr	3.3–11.4	1.7–2.7	4.0–11.0
	Fe	3.3–16.6	1.7–2.6	4.0–16.5
	Ni	3.3–16.7	1.7–2.6	4.0–16.5
SUS304	Cr	3.3–11.4	1.7–2.7	4.0–11.0
	Fe	3.2–16.7	1.7–2.6	4.0–16.5
	Ni	3.3–16.7	1.7–2.6	4.0–16.5

$[C_2 = \langle (r-R)^2 \rangle]$, C_3 is the mean cubic relative displacement $[C_3 = \langle (r-R)^3 \rangle]$, S_0^2 is the intrinsic reduction factor due to the many-electron effect, $F(k)$ is the backscattering amplitude including the inelastic scattering loss factor, and $\phi(k)$ is the total phase shift between the x-ray absorbing and photoelectron scattering atoms.

For the curve-fitting analysis to obtain the structural parameters, theoretical standards were at first calculated using FEFF8.4 [14]. Here we assumed randomly distributed clusters with the fcc lattice constant of 3.57129 Å (the number of the fcc unit lattices of 4^3 and the total number of atoms of $4 \times 4^3 = 256$), where the composition ratios of the Elinvar and SUS304 alloys were assumed to be $Fe_{52.2}Ni_{42.4}Cr_{5.4}$ (Ti neglected) and $Fe_{72}Ni_9Cr_{19}$ (Mn neglected), respectively. Ten random alloy clusters were evaluated and the average EXAFS spectra were obtained as consequent theoretical standards. Although static lattice strains are actually expected in these alloys, the FEFF simulations were conducted with the assumption that all the atoms are distributed at ideal lattice positions. Note here that the neighboring atoms around the x-ray absorbing atom cannot be distinguished because of only small differences of the backscattering amplitudes among Fe, Ni, and Cr, and therefore the resultant values obtained experimentally are regarded as the average one for each x-ray absorbing atom.

The curve-fitting analysis of the experimental EXAFS spectra at 20 K was subsequently performed using the FEFF standards obtained above. Here the parameters fitted were S_0^2, R, ΔE_0 (edge energy shift), and C_2 (fixed at $N = 12$ and $C_3 = 0$). The fitting results are summarized in Table II. Finally, the curve-fitting analysis of all the EXAFS spectra were carried out using the results of 20 K as empirical standards, with the assumption that S_0^2, N, and ΔE_0 are identical to the ones at 20 K, while R, C_2, and C_3 are fitting variables.

B. PIECP MC simulations

PIECP MC simulations within the low coupling approximation [11] were performed under constant number of particles, pressure, and temperature (NPT) condition. Although the PIECP theory can treat only periodic lattices [11] and is strictly not applicable to the present random alloy systems, the Elinvar and SUS304 alloys exhibit clear fcc structure and the atomic weights of Cr, Fe, and Ni are not very different, allowing us to adopt the theory to the present simulations of alloy systems. This assumption was found to work well in our previous studies [5,6]. The potentials of Fe, Ni, and Cr are based on the empirical embedded-atom method (EAM) [15,16]. In the EAM, the total energy E of the system is given as

$$E = \sum_i \mathcal{F}_i(\rho_{h,i}) + \frac{1}{2} \sum_i \sum_{j \neq i} \phi_{ij}(R_{ij}), \tag{2}$$

where the electron density of the surrounding atoms $\rho_{h,i}$ is expressed as

$$\rho_{h,i} = \sum_{j \neq i} \rho_j^a(R_{ij}). \tag{3}$$

The first and second terms in Eq. (1) correspond to the metallic bondings with valence electrons and the repulsion between ion cores, respectively. The numerical parameters of AFM Fe, Ni, and Cr employed were referred to the literature [17]. In Fe, the energy difference between the FM and AFM states were evaluated by referring to the literature [18], where the difference $\mathcal{F}_i^d(\rho_{h,i}^d)$ between the FM and AFM states is given as a function of the d-electron density $\rho_{h,i}^d$ of all the surrounding atoms at each Fe site:

$$\mathcal{F}_i^{\rm d}(\rho_{h,i}^d) = \mathcal{F}_i^{\rm FM}(\rho_{h,i}) - \mathcal{F}_i^{\rm AFM}(\rho_{h,i}). \tag{4}$$

The potential parameters are tabulated in the Supplemental Material [19]. For comparison, the MC simulations based on the classical thermodynamics were also carried out.

The total number of atoms was 500 (5^3 fcc cubic unit cells), and the distributions of Fe, Ni, and Cr were chosen randomly. In a similar manner to the FEFF evaluations, ten types of the superlattices were simulated and the results were averaged to provide consequent physical quantities. The MC simulations were performed based on the conventional Metropolis method, where 100 000 MC steps were calculated with 500 time trials of the atom movement and one trial of the lattice constant variation in each MC step. In the calculations of structural quantities, the results before the system reaches sufficient equilibrium (∼10 000 MC steps at high temperature and

TABLE II. Results of the EXAFS analysis for the first-NN shells in Elinvar alloy and SUS304 determined by the Cr, Fe, and Ni K-edge EXAFS at 20 K.

Sample	Edge	S_0^2	R (Å)	ΔE_0 (eV)	C_2 (10^{-2}Å^2)	R factor	χ_ν^2
Elinvar	Cr	0.707(9)	2.5072(8)	0.08(16)	0.333(9)	0.009	3.1
	Fe	0.774(8)	2.5300(5)	−0.28(14)	0.369(5)	0.012	3.5
	Ni	0.779(7)	2.5304(5)	−0.15(14)	0.341(5)	0.009	1.5
SUS304	Cr	0.632(9)	2.5114(8)	−0.24(17)	0.321(10)	0.014	5.8
	Fe	0.779(8)	2.5261(5)	−0.06(14)	0.350(5)	0.035	38.4
	Ni	0.706(6)	2.5302(4)	0.24(12)	0.207(3)	0.060	31.4

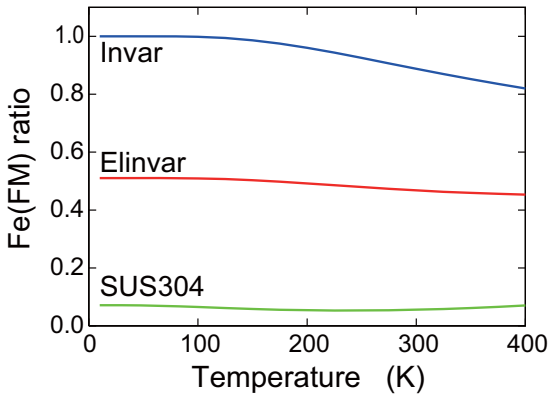

FIG. 5. FM Fe ratios in Invar, Elinvar, and SUS304 alloys as a function of temperature, estimated by the present PIECP MC simulations.

~50 000 MC steps at low temperature) were excluded. The temperatures considered in the present simulations were in the range of 10–400 K.

Figure 5 shows the ratios of FM Fe as a function of temperature estimated in the present PIECP MC simulations. In the Invar alloy reported previously [5], the FM Fe ratio decreases with the temperature rise, which results in the Invar effect. In the Elinvar alloy, the ratio is found to be rather small even at low temperature and be reduced a little at higher temperature, while in SUS304 the ratio is quite small for all the temperature range, implying that almost all the Fe atoms in SUS304 are in the AFM state. In the present simulations, the stabilities of FM and AFM Fe are dependent on the d-electron densities of the surrounding atoms at the central Fe site; the AFM state is more stable if the d-electron density is larger. Although the number of d electrons increases with the atomic number (Cr < Fe < Ni), the d-electron density of the surrounding atoms depends more strongly on the radial distribution of the atomic wave function and the resultant sequence is Ni < Fe < Cr, implying that the Fe atom with more surrounding Ni atoms favors FM, while that with more surrounding Cr is likely to exhibit AFM.

III. RESULTS AND DISCUSSION

Figure 6 shows temperature dependence of the first-NN interatomic distances determined by the present EXAFS analysis, together with the estimated values from the lattice constant given by the x-ray diffraction (Fig. 2) and the present PIECP MC simulations. The local linear thermal expansions are summarized in Table III, which were evaluated as the gradients of the curves in Fig. 6 between 80 and 300 K. A clear difference can be seen in temperature dependence of the interatomic distances around Fe between Elinvar and SUS304; the local thermal expansion around Fe in the Elinvar alloy is noticeably smaller than that in SUS304; those of the Elinvar and SUS304 alloys are 1.33×10^{-5} and 2.39×10^{-5} (Å/K), respectively. Although in Fig. 6 the thermal expansions around Ni or Cr do not differ so much between the Elinvar and SUS304 alloys, the local thermal expansions around Ni and Cr in Elinvar are found to be slightly smaller than the corresponding ones in SUS304,

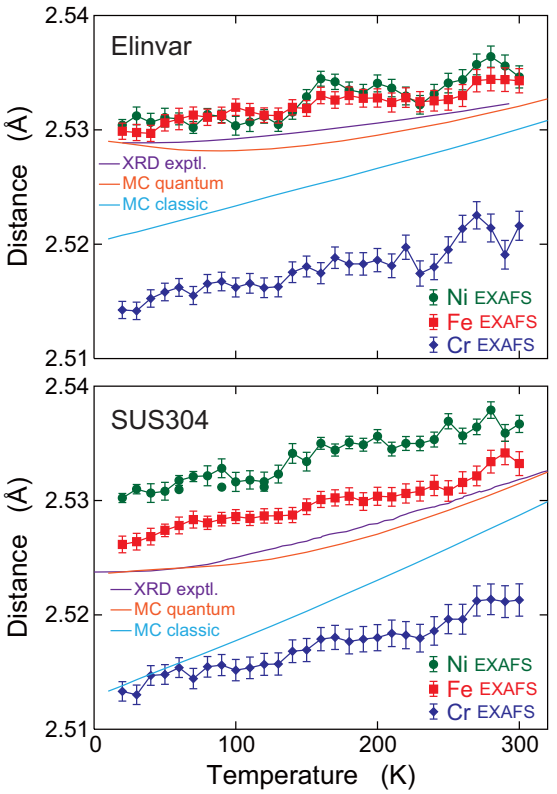

FIG. 6. Temperature dependence of the first-NN interatomic distances in the Elinvar and SUS304 alloys. The results of the Fe, Ni, and Cr K-edge EXAFS analysis are given, together with the results of the lattice constant (divided by $\sqrt{2}$) determined from the powder x-ray diffraction (purple solid line) and the calculated results obtained by the present PIECP (orange solid lines) and the classical (light blue solid lines) MC simulations.

as seen in Table III. This indicates that in the Elinvar alloy the Invar effect occurs dominantly around Fe and somewhat influences the local structures around Ni and Cr as well.

The thermal expansions given as gradients of the curves in Fig. 6 are found to be in good agreement with the results of x-ray diffraction and the present PIECP MC simulations, and the local thermal expansion around Fe in the Elinvar alloy estimated by the PIECP MC simulations is smaller than the one in SUS304. On the other hand, the calculated results in the classical MC simulations exhibit linear thermal expansion, as is expected in the simple classical thermodynamic theory, and they are a little too large compared with the experimental data and the PIECP results. This indicates that the vibrational quantum effect of the finite zero-point vibrational amplitude is quite important at low temperature. It is also found that in both

TABLE III. Linear local thermal expansions around Cr, Fe, and Ni in the Elinvar and SUS304 alloys determined by the EXAFS analysis (given as the unit of 10^{-5} Å/K).

Sample	Cr	Fe	Ni
Elinvar	2.32	1.33	2.17
SUS304	2.85	2.39	2.40

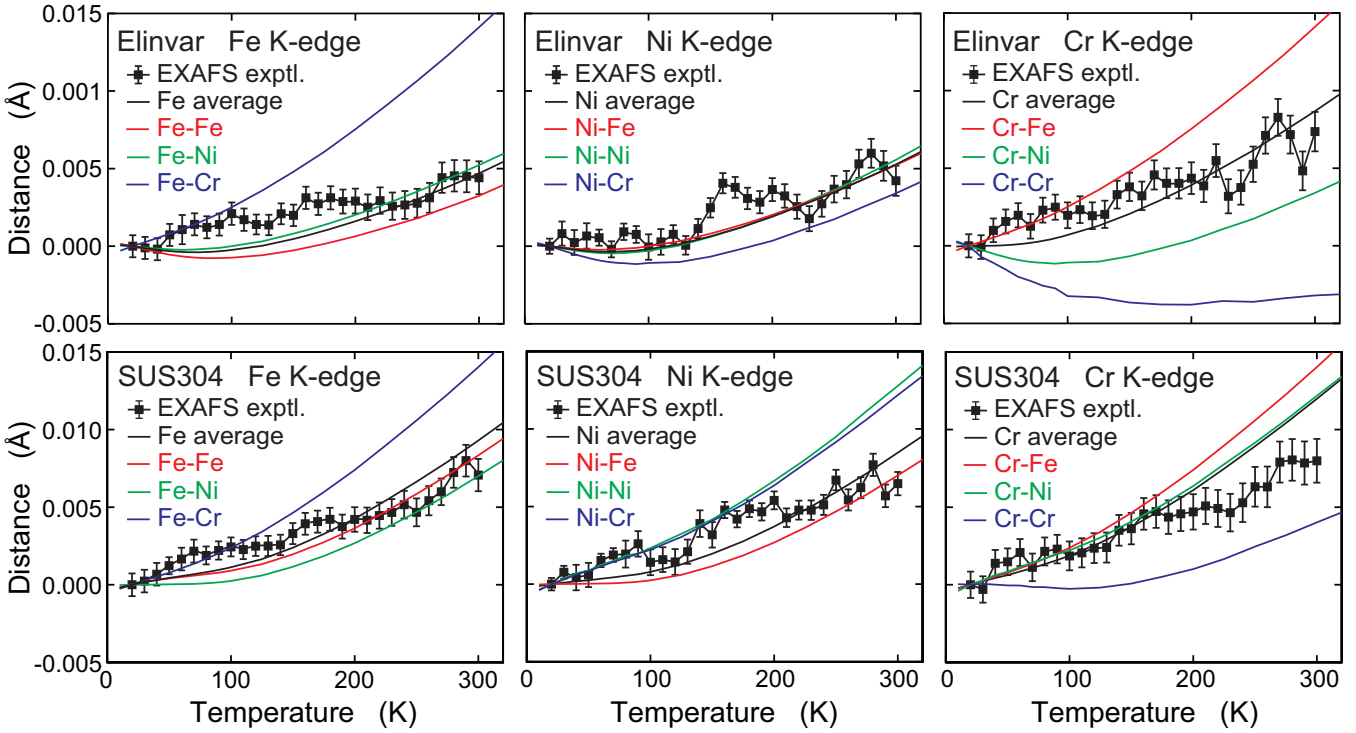

FIG. 7. Temperature dependence of the first-NN interatomic distance for each atom pair in the Elinvar and SUS304 alloys estimated by the PIECP MC simulations. The variations with respect to the value at 20 K are given. The EXAFS results are also depicted for comparison.

the alloys the interatomic distance around Cr is considerably shorter than those around Fe and Ni, implying the presence of large strains of the fcc lattice around Cr. Although both the alloys show fcc lattices from the average periodic point of view, the local strains and the difference in the local thermal expansions are clearly observed in the EXAFS analysis from the local point of view.

Figure 7 shows the first-NN interatomic distances of each atom pair estimated from the PIECP MC simulations. Here the difference from the values at 20 K is plotted, together with the average distance obtained by the experimental EXAFS analysis. The EXAFS results are mostly in good agreement with the average results obtained by the PIECP MC simulations, indicating high reliability of the present PIECP MC simulations. In the Elinvar alloy, the local thermal expansion for the Fe-Fe pair is actually quite small, which is a reasonable consequence in the incomplete Invar-like effect. The local thermal expansions of the Ni-Cr, Fe-Ni, and Ni-Ni pairs are also rather small, indicating the influence of the Invar effect that occurs dominantly around Fe. The most interesting and

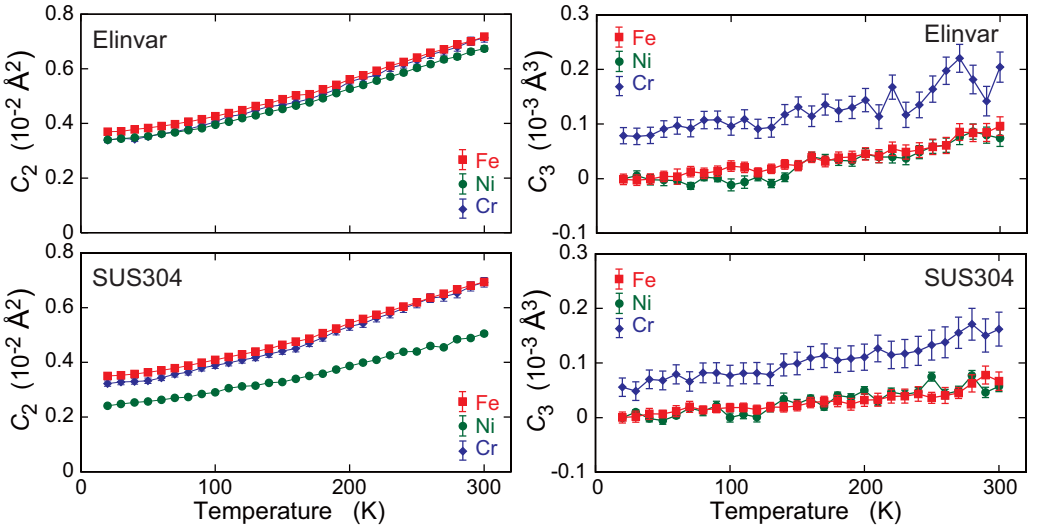

FIG. 8. Temperature dependence of the mean square relative displacements C_2 and the mean cubic relative displacements C_3 for the first-NN shells in the Elinvar and SUS304 alloys obtained by the EXAFS analysis.

peculiar findings in Fig. 7 may be that the thermal expansion in the Cr-Cr pair is negative at low temperature (<150 K) and shows the Invar-like effect, while that in the Cr-Fe pair seems extraordinarily large. These findings are in good accordance with the EXAFS results, where the lattice strains take place dominantly around the Cr atoms. Also in SUS304, where no Invar effect should be expected, the local thermal expansions for the Cr-Cr and Cr-Fe pairs are found to be abnormally small and quite large, respectively, implying the significant strains around Cr to maintain the lattice also in the SUS304 alloy. Although the reason why the strains are concentrated in Cr is not clear, it can be supposed that the Cr atoms favor bcc lattices and are the most unstable among the three elements of Cr, Fe, and Ni that form fcc alloys.

Finally, Fig. 8 shows the mean square relative displacements C_2 and the mean cubic relative displacement C_3 for the first-NN shells for the Elinvar and SUS304 alloys obtained by the EXAFS analysis. As in the previous study on the Invar alloy [5], we observed sufficiently large C_3, implying that the asymmetric radial distribution due to vibrational anharmonicity is strictly present even in the system with very small thermal expansion like the Elinvar alloy. We tried to fit the observed C_2 values using the correlated Debye model [20]. The fitness was however found to be poor, because the observed C_2 exhibits gradual increase even at low temperature, while the Debye model shows a convergence at low temperature to yield the zero-point vibrational displacement. Although the reason is not clearly understood and further studies are hopefully performed, it is supposed that the static disorder in the Elinvar and SUS304 alloys is temperature dependent.

IV. CONCLUSIONS

We have measured temperature dependent Cr, Fe, and Ni K-edge EXAFS spectra of the Elinvar and SUS304 alloys combined with the PIECP MC theoretical simulations in order to investigate local thermal expansions and lattice strains. The EXAFS analysis clarifies that in the Elinvar alloy the local thermal expansion around Fe is considerably smaller than the ones around Ni and Cr. This observation is associated with the fact that Fe in the Elinvar alloy exhibits the incomplete Invar-like effect. In both the Elinvar and SUS304 alloys, the local thermal expansions and the lattice strains around Cr are found to be significantly larger than the ones around the other elements. The PIECP MC simulations of both the alloys further elucidate that the first-NN Cr-Fe pair gives extraordinarily large thermal expansion, while the Cr-Cr pair provides quite small or even negative thermal expansion. These findings consequently indicate that the lattice strains in both the Elinvar and SUS304 alloys are concentrated dominantly on the Cr atom sites.

It is well known that the role of Cr in stainless steel is to inhibit corrosion by the formation of surface chromium oxide. The present investigation may interestingly suggest that the Cr atoms in the bulk play a hidden new role of absorbing inevitable lattice strains in the alloy. The present study demonstrates that the local thermal expansions and the lattice strains clearly differ from the ones simply expected from the average crystallographic lattices and that the local structure determination using EXAFS is essentially important to understand the detailed structural nature of alloys and mixed crystals.

ACKNOWLEDGMENTS

We would like to thank Dr. H. Abe in KEK-PF for his help during the EXAFS measurements. We are grateful for the partial financial support by JSPS (Japan Society for the Promotion of Science) KAKENHI Grant Number JP15H02173. The EXAFS measurements at Photon Factory have been performed under the approval of Photon Factory Program Advisory Committee (PF-PAC Proposal No. 2017G034).

[1] J. B. Boyce and J. C. Mikkelsen, Jr., Phys. Rev. B **31**, 6903(R) (1985).
[2] J. C. Mikkelsen, Jr. and J. B. Boyce, Phys. Rev. B **28**, 7130 (1983).
[3] R. A. Mayanovic, W.-F. Pong, and B. A. Bunker, Phys. Rev. B **42**, 11174 (1990).
[4] H. Sato, T. Yokoyama, I. Ono, K. Kaneyuki, and T. Ohta, Jpn. J. Appl. Phys. **31**, 1118 (1992).
[5] T. Yokoyama and K. Eguchi, Phys. Rev. Lett. **107**, 065901 (2011).
[6] T. Yokoyama and K. Eguchi, Phys. Rev. Lett. **110**, 075901 (2013).
[7] C. E. Guillaume, CR Acad. Sci. **125**, 235 (1897).
[8] R. J. Weiss, Proc. R. Soc. Lond. A **82**, 281 (1963).
[9] W. S. McCain and R. Maringer, *Mechanical and Physical Properties of Invar and invar-Type Alloys* (Battel Memorial Institute, Defense Metals Information Center, Columbus. OH, 1965).
[10] Y. S. Touloukiun, R. E. Kirby, R. E. Taylor, and P. D. Desai, *Thermophysical Properties of Matter Vol. 12, Thermal Expansion Metallic Elements and Alloys* (Plenum, New York, 1975).
[11] A. Cuccoli, R. Giachetti, V. Tognetti, R. Vaia, and P. Verrucchi, J. Phys.: Condens. Matter **7**, 7891 (1995).
[12] T. Yokoyama, Phys. Rev. B **57**, 3423 (1998).
[13] http://pfxafs.kek.jp/beamline/bl9c/
[14] A. L. Ankudinov, A. I. Nesvizhskii, and J. J. Rehr, Phys. Rev. B **67**, 115120 (2003).
[15] M. S. Daw and M. I. Baskes, Phys. Rev. B **29**, 6443 (1984).
[16] S. M. Foiles, Phys. Rev. B **32**, 3409 (1985).
[17] G. Bonny, N. Castin, and D. Terentyev, Model. Simul. Mater. Sc. **21**, 085004 (2013).
[18] S. L. Dudarev and P. M. Derlet, J. Phys.: Condens. Matter **17**, 7097 (2005).
[19] See Supplemental Material at http://link.aps.org/supplemental/10.1103/PhysRevMaterials.2.023601 for the EAM potential parameters employed in the present simulations.
[20] G. Beni and P. M. Platzman, Phys. Rev. B **14**, 1514 (1976).